Applied Surface Science 514 (2020) 145926

Contents lists available at ScienceDirect

Applied Surface Science

journal homepage: www.elsevier.com/locate/apsusc

Full Length Article

Synthesis of graphene-related carbon nanoparticles from a liquid isopropanol precursor by a one-step atmospheric plasma process

W. Bodnar[a,*], M. Schiorlin[a], A. Frank[b], T. Schulz[a], N. Wöhrl[c], C. Miron[a,d], C. Scheu[b,e], J.F. Kolb[a], A. Kruth[a]

[a] Leibniz Institute for Plasma Science and Technology, Felix-Hausdorff-Str. 2, 17489 Greifswald, Germany
[b] Max Planck Institute for Iron Research GmbH, Max-Planck-Str. 1, 40237 Düsseldorf, Germany
[c] University of Duisburg-Essen, Faculty of Physics and CENIDE, Lotharstr. 1, 47057 Duisburg, Germany
[d] Shibaura Institute of Technology, 3 Chome-7-5 Toyosu, Koto-ku, Tokyo 135-8548, Japan
[e] RWTH Aachen University, Materials Analytics, Kopernikusstr. 10, 52074 Aachen, Germany

ARTICLE INFO

Keywords:
Nanographite
Graphene
Plasma-in-liquid
Raman spectroscopy
Transmission electron microscopy
Gas chromatography - mass spectrometry

ABSTRACT

This study presents a cost-efficient single-step-method to synthesize nanographite from isopropanol by bipolar pulsed electric discharges. The influence of pulse width within the nanosecond range, repetition frequency within the kilohertz range and processing time on the product was systematically investigated by Raman spectroscopy, high-resolution transmission electron microscopy and gas chromatography - mass spectrometry. It was found that long pulses in the microsecond range promote the creation of amorphous and oxidic carbon structures. Although, hydrocarbon cracking and subsequent graphitization do occur, these process conditions are not suitable to drive intermediate reduction processes. In contrast, applying short pulses in the nanosecond regime ensures fast reduction processes and formation of graphene-related nanostructures. The number of observed nanographite layers lies in the range of 3–13 with an average interlayer spacing of 3.4(0.3) Å and an average distance between defects of 11.5(6.0) nm meaning that the produced nanographite is in the area of small defect density. Furthermore, no significant influence of process times on the product properties over a period up to 15 min was observed, indicating good process homogeneity.

1. Introduction

Nanostructured carbon materials such as graphene, multi-layer graphene, graphene oxide or carbon nanotubes have attracted considerable attention in the recent years due to their unique physical properties [1–4]. Single and multi-layer graphene can be used in a great variety of applications such as conductive wires for transparent touch panels, for conductive inks, in sensors, as anti-corrosion coating, for heat dissipation in films or pastes, for battery electrodes, as a material for supercapacitor electrodes, or as a catalyst support in proton exchange membrane fuel cells [1,4–8].

Cost-efficient production of contamination-free graphene for electronic and electrochemical applications at an industrial scale is still a big challenge which demands the development of novel manufacturing methods [9]. Few layer graphene can be prepared by mechanical exfoliation of small mesas of highly oriented pyrolytic graphite [10]. However, this method is not applicable for a large-scale production. Graphene has also been prepared by various other methods, e.g. heating of SiC [11,12], intercalation followed by sonication [13], interaction with polar solvents [14,15], plasma enhanced chemical vapor deposition [16,17], thermal exfoliation of graphite oxide [18,19], conversion of nanodiamond in an inert atmosphere at high temperatures [19,20], growth on metallic substrates (e.g. Ni, Cu) by chemical vapor deposition [21] or gas-phase synthesis in a microwave plasma reactor from ethanol [22]. In all of the reported cases, the quality of the product and the number of achieved layers varies strongly, depending on the applied method.

Especially, the liquid phase exfoliation has been recognized in recent years for its potential of a large scale production of graphene [23]. This method is cost-efficient and scalable for industrial applications. Graphene layers in graphite are bound only by weak van der Waals forces [24]. These bonds can be broken during a liquid phase exfoliation process, using a suitable medium. Examples are *N*-methylpyrrolidone and *N*,*N*-dimethylformamide which also stabilize the suspension [23,25]. Initially, liquid phase exfoliation was mainly performed using toxic and expensive solvents, without a need for any further surfactants.

* Corresponding author.
E-mail address: wiktor.bodnar@inp-greifswald.de (W. Bodnar).

https://doi.org/10.1016/j.apsusc.2020.145926
Received 3 October 2019; Received in revised form 23 February 2020; Accepted 26 February 2020
Available online 27 February 2020
0169-4332/

A major recent improvement has been the successful introduction of water as a solvent [25] even though the surface energy of water itself is not suitable for exfoliation. Therefore, aromatic, non-aromatic or ionic liquids, as well as polymer based surface-active substances had to be added. However, graphene produced in such way is characteristic of a poor quality and only a small yield is obtained, thus this method is not suitable for electrochemical applications [25].

Chemical vapor deposition and thermal decomposition of carbides are mainly applied and further developed for obtaining graphene monolayers on substrates for electronic applications [26–29]. However, the control of the process parameters on a large-scale in these methods is problematic not only due to the evaporation of the substrates at temperatures of approximately 1000 °C, but also due to the high activation energy for the catalytic reaction [26,28].

Although a wide variety of synthesis methods of graphene production is available, most of these methods have small synthesis rates, high processing costs and they require rather large equipment. Therefore, in the recent years novel approaches have been proposed.

For electrochemical exfoliation, a graphite electrode is oxidized and negative ions of the electrolyte are intercalated between graphene layers in the graphite crystal [30]. The selection of the electrolyte is critical. Mainly, water solutions of different inorganic salts, e.g. $(NH_4)_2SO_4$, Na_2SO_4 or K_2SO_4 are used [31]. The exfoliation does not only take place at the surface of the graphitic electrode, but especially in the bulk. Therefore, larger graphite crystals are present in the product. The fraction of larger graphite crystallites significantly increases with the increasing surface area of the graphite electrode.

A promising, cost-efficient and environmentally friendly single-step-approach is the so-called plasma-in-liquid (PiL) method [32–34]. PiL methods involve discharges between electrodes directly submerged in liquid, as well as discharges at the interface of a bulk liquid and a gas phase. It has already been reported that electric discharges between electrodes in hydrocarbons yield nanographite or few layer graphene [35–37]. In the plasma-in-liquid synthesis electrons with high kinetic energies and active chemical species such as ions, radicals and metastable atoms are produced. Different types of discharges, namely corona, arc or streamers, can be generated in various solvents and liquid precursors depending on the process parameters [32–34]. The occurrence of different discharges resulting in different products, is related to the pulse length, frequency, applied voltage and current, as well as the distance between electrodes.

Diamond-like nanocarbons were synthesized in Ar gas bubble discharge in ethanol using a reactor with tip-to-plate configuration. Ar bubbles were injected through the hollow tip electrode. Pulsed discharges in a nanosecond range were generated with a high voltage pulse generator with +9 kV at the anode mesh electrode and −9 kV at the cathode needle electrode. The gas flow rate through the hollow needle with an inner diameter of 0.44 μm was 100 sccm. The ethanol was dissociated at the liquid-gas interface into C2 and CH reactive species, which are primary species for nanocarbon formation. The synthesized product was found to have three main features, namely amorphous carbon spheres, lonsdaleite (nano-diamond) spheres and graphitic carbon shrouds [38].

Carbon nanoparticles have been synthesized using a tip-to-tip geometry applying bipolar pulses and using an additional external resistor to minimize unstable discharges. The carbon nanoparticles were synthesized directly from different aliphatic precursors. 5 kHz bipolar pulses were used in the driving circuit, and an inverter amplified the low primary voltage. An external resistor of 1 kΩ was applied to obtain stable discharges. Two tungsten wires with 1.2 mm diameter and covered with polytetrafluoroethylene were used as electrodes with a gap of 1 mm between them. A magnetic stirring bar was inserted into the reaction chamber in order to reduce particle aggregation. Six aliphatic n-alcohols (methanol to hexanol) were used to compare the obtained carbon nanoparticles. The synthesis rate of carbon nanoparticles increased with increasing carbon ratios in alcohol. Nevertheless, the size of the nanoparticles decreased. The degree of graphitization of the particles increased when the carbon to oxygen ratio was high [39]. Furthermore, defective nanographite with less than 100 nm was obtained using a PiL setup with a tip-to-tip configuration in ethanol using graphite rods as electrodes with a diameter of 3 mm. The gap between electrodes was 1 mm and a pulsed voltage of 4 kV was applied. The frequency and the pulse width of the unipolar pulses were 30 kHz and 4 μs, respectively. A magnetic stirrer was used during the synthesis [7]. It also has been reported that nanographite was synthesized using pulsed discharges at an ethanol - argon interface. A tip-to-plate geometry was used in which the tip was made of tungsten and the plate of molybdenum. Monopolar pulsed discharges with three different frequencies of 1, 3 and 5 kHz, were applied. At 1 kHz, the peak voltage was 6.5 kV and the peak current of the discharge was 7 A. At 3 kHz and 5 kHz, the peak voltage and the peak current were 4.3 kV and 5.4 A, as well as 3.2 kV and 2.4 A, respectively. The deposition rate of nanographite was 3.2 mg/min at 1 kHz, 2.5 mg/min at 3 kHz and 1.3 mg/min at 5 kHz. With the increasing frequency, the domain size of the nanographite reduced from 34 nm to 19 nm and the number of layers decreased significantly [35].

High-speed synthesis of highly crystalline nanographite was performed with butanol and ethanol as precursors. A reactor with tip-to-plate configuration was used. The tip electrode had a microhollow structure at its edge enabling the generation of ultrahigh electron densities in the microhollow region. An alternating voltage of 9 kV with a frequency of 60 Hz was applied between electrodes, creating a sequential discharge between the ultrahigh-density plasma and the lower electrode through the gas-liquid interface. After 15 min of discharge, a black precipitate was obtained in the suspension. It was filtered using hydrogen peroxide in order to remove byproducts such as amorphous carbon. The synthesis rates of nanographite from ethanol and butanol were 0.61 mg/min and 1.72 mg/ml, respectively [36]. The same experiments were performed using ethanol, propanol and butanol and a voltage of 10 kV. In this case the synthesis rates were 0.34 mg/min, 0.67 mg/min and 1.00 mg/min, respectively [40]. Furthermore, nanographite was synthesized in ethanol using a PiL setup with a tip-to-plate configuration. Both electrodes were made of Cu and the generation of nanographite took place at the gas-liquid interface between argon and ethanol using alternating high voltage. The obtained product was directly filtered using hydrogen peroxide at 80 °C in order to remove amorphous carbon from the product [8].

Moreover, graphite nanosheets consisting of many folds and curled edges with up to 11 μm in extent and a thickness of 6.7–23.5 nm could be obtained using low-current plasma discharges in ultrasonically cavitated liquid ethanol. A rod with a diameter of 3 mm made of Fe-Pt alloy (50–50%) served as an anode and the cathode was an Fe plate mounted on an ultrasonic horn. The voltage between the anode and the cathode was kept at 55 V and the upper limit of the current was 3 A. The effervescent ultrasonic cavitation field was used to enhance electrical conductivity due to formation of high-energy species like radicals, atoms, ions and free electrons. Graphite nanosheets and Fe-Pt alloy filled carbon nanocapsules were identified in the final product [41]. Detailed analysis of the synthesized particles allowed the determination of a possible reaction pathway being a dissolution-precipitation process of the carbon species in the Fe-Pt alloy nanoparticle. Evaporation of the Fe-Pt anode and decomposition of ethanol molecules by the plasma discharge take place simultaneously leading to a reaction between metallic vapor and the carbon species. Liquid Fe-Pt-C alloy particles are formed in close proximity to the plasma discharge zone. During the dissolution of the released carbon species in the liquid Fe-Pt-C particles, the particles become saturated with carbon according to the carbon solubility limit. Therefore, carbon segregation begins during the quenching by the surrounding liquid ethanol. Thus, graphene layers form at the outer surface of the Fe-Pt alloy nanoparticles [42].

In this study, a novel PiL-dedicated bipolar pulse generator was used which is based on new SiC power devices enabling short pulse lengths

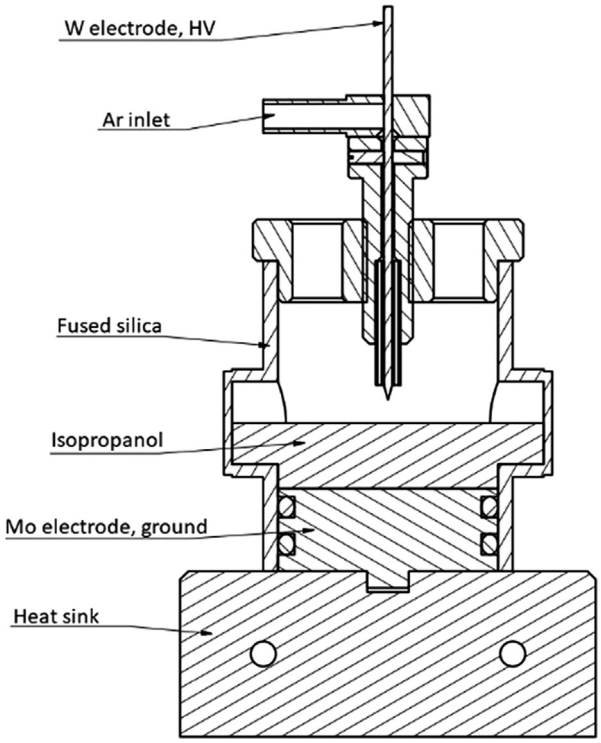

Fig. 1. Scheme of the experimental reactor for PiL synthesis in a tip-to-plate configuration.

from nanoseconds to microseconds and high repetition frequencies in the kilohertz regime. Therefore, it was possible to demonstrate a direct influence of the PW and RF varied in the wide rage on the product, starting from amorphous structures, graphene oxides to nanographite. Preferences with respect to anode and cathode processes could be leveraged by the bipolar high voltage pulses and accordingly also selective electrode erosion [33,43]. The short high voltage pulses promote electron collision dominated reaction mechanisms, while longer pulses contribute increasingly to thermal processes. The high repetition rates are a prerequisite for fast processing times. Successful operating parameters to obtain different types of graphene-related carbon nanoparticles, especially nanographite, are determined by the quality and the yield of the product that was formed from the isopropanol.

2. Experimental

2.1. Reactor and pulsed discharge generator

A reactor for PiL synthesis of carbon nanoparticles from a liquid precursor in a tip-to-plate electrode configuration was built in-house according to the schematics presented in Fig. 1. The reaction chamber of the reactor was made of fused silica and it can contain a maximum volume of 50 ml of liquid precursor. A tungsten rod with a diameter of 2 mm was used as the high voltage (HV) electrode. The HV electrode was centered in a ceramic tube for insulation, which also acted as a gas inlet. The ground electrode with a diameter of 55 mm was made of molybdenum and connected to a water-cooled heat sink in order to control the process temperature.

Pulsed electric discharges (PD) were generated by means of a Pekuris MPP-HV04 bipolar pulse modulator for PiL from Kurita Manufacturing Corporation, Ujitawara, Kyoto, Japan. This generator provides bipolar high voltage pulses of up to 10 kV with a pulse width (PW) up to 1.6 µs and a repetition frequency (RF) ranging from 2 kHz up to 200 kHz.

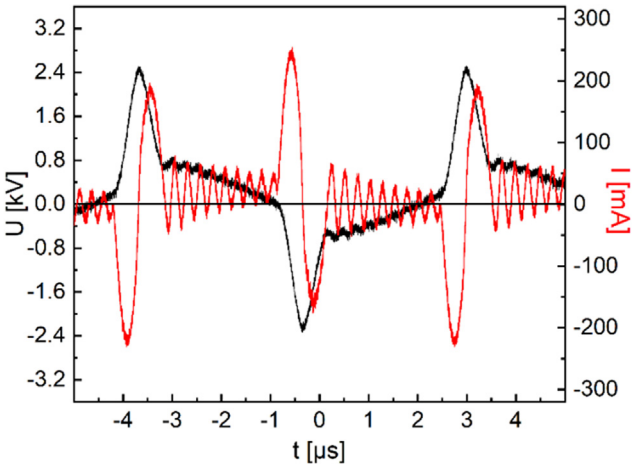

Fig. 2. Exemplary I-U characteristics of the Kurita Pekuris MPP-HV04 bipolar PD generator with an external load.

2.2. Synthesis

Synthesis was performed using a volume of 20 ml of isopropanol (purity ≥ 99.5%, Carl Roth GmbH) as a carbon precursor. The reactor was filled with the alcohol and placed in a chamber allowing for evacuation of ambient laboratory air and providing an inert gas atmosphere. Prior to the experiments, the chamber was evacuated and flushed with high purity Ar three times. The pressure during the synthesis was kept at 0.8 bar with an Ar flow of 100 sccm. The temperature of the heat sink was set to 10 °C. The distance between the HV and the ground electrodes was 14 mm, with 4 mm between the HV electrode and the surface of the isopropanol.

Carbon products were prepared applying three different pulse widths, i.e. PW = 320 ns, 1.1 µs and 1.6 µs, and with four different repetition frequencies, i.e. RF = 60, 110, 150 and 200 kHz. In all cases, a stable glow-like discharge in Ar over the liquid surface with intense streamer-like discharges reaching into the liquid were established at an initial voltage of 1.7 kV. The target operating voltage was set to 2.5 kV and the processing time was 3 min. A typical current- voltage (I-U) characteristics of the bipolar PD generator with an external load during the synthesis is shown in Fig. 2. The current-voltage characteristics for different operating parameters are determined by the equivalent RCL-circuit elements that are describing the pulse generator and the reaction chamber.

In order to investigate the influence of the processing time on the yield and the composition of the resulting product, a series of samples was prepared applying PW = 320 ns and RF = 150 kHz, at varying processing times. In order to determine the yield of the solid product, the obtained suspensions were drop-casted onto pre-weighted aluminum dishes, dried in an oven for 4 h at 60 °C and then weighted using a Sartorius CCE 06 microbalance.

2.3. Raman spectroscopy

Raman spectra were collected with a Renishaw inVia spectrometer within the wavenumber ranging from 900 to 3200 cm^{-1} using a Nd-YAG laser with an excitation wavelength of 532 nm. Prior to measurements, the suspensions were deposited onto Si(1 0 0) polished wafers and then dried at room temperature. The obtained spectra were normalized and fitted using WiRE software from Renishaw assuming Voigt peak profiles.

2.4. STEM and EDX

For scanning transmission electron microscopy (STEM)

investigations the suspensions have been drop-casted onto carbon coated gold grids without further modifications and dried at room temperature. High-resolution TEM (HRTEM) was performed using a FEI Titan Themis operating at 300 kV and equipped with a Cs-image corrector. For STEM investigations and energy-dispersive X-ray spectroscopy (EDX) a FEI Titan Themis operating also at 300 kV with an attached Cs-probe corrector was used. This machine has a Super-X windowless EDX system with four synchronized silicon drift detectors from Bruker, allowing for EDX measurements with very high count rates. In order to exclude influences of the TEM grid material on the EDX measurements, additionally a sample on a carbon coated copper grid was investigated.

2.5. GC–MS

Gas chromatography - mass spectrometry (GC–MS) was applied to analyze residual liquids of the synthesized suspensions. After filtration of the liquids, 1 µl of the solution was injected into the GC–MS system, which was Agilent 7860B with Agilent HP-5 ms column (30 m length, 0.25 mm diameter, 0.25 µm film thickness) coupled with Agilent 5973-MSD mass spectrometer. The temperature of the oven was varied from 40 °C to 300 °C in a two-step program, the temperature of the injector was set to 300 °C and the transfer line was heated to 300 °C. The temperature of the MS source and of the quadrupole were 230 °C and 150 °C, respectively.

3. Results and discussion

3.1. Influence of repetition frequency and pulse width on product characteristics

The Stokes phonon energy shift caused by a laser excitation with 532 nm creates two main bands in the Raman spectrum of pristine graphene. Namely, a primary in-plane vibrational mode G at 1580 cm^{-1} and a second-order overtone of a different in-plane vibration 2D(G′) at 2690 cm^{-1} [44]. As the number of graphene layers increases, the spectrum undergoes changes. The 2D(G′) band becomes wider, less intensive and shifts to higher frequencies while the G band shifts to lower energies [45,46]. Furthermore, typical spectra feature also signatures from defects and disorder in the graphite/graphene crystal. The most prominent are the D band (~1200–1400 cm^{-1}), the D′ band (1600–1630 cm^{-1}) and the (D + D′) band (~2950 cm^{-1}) [47].

Fig. 3 presents Raman spectra of the samples synthesized by PiL from isopropanol using a bipolar-pulsed electric discharge with different pulse widths and repetition frequencies. A decrease of the pulse width as well as an increase of the repetition frequency lead to significant changes in the spectra. Samples prepared with PW = 1.6 µs seem to be dominated by a defective partially reduced graphene oxide [2], while samples prepared with PW = 320 ns show a structure more typical for nanographite or few layer graphene [45,46]. The most noticeable change of the Raman spectra in Fig. 3 is an increase of the intensity of the 2D(G′) band, which corresponds to a decrease of the number of nanographite layers [44–46]. Moreover, small changes of its shape and position can be noticed. Presumably, this is due to the fact that the samples prepared by PiL at longer PW and lower RF contain not only nanographite or graphene oxide but also different products like amorphous carbon or soot [48,49], so the bands originated by different components may partially overlap. At the same time, the intensity of the (D + D′) band at ~2950 cm^{-1} is reduced compared to the 2D(G′) band for shorter PWs suggesting a better quality of the nanographite flakes.

Fig. 4 shows the intensity ratios I_D/I_G, as well as I_{2D}/I_G, for samples synthesized with different PWs and RFs. The integrated intensity ratios I_D/I_G and I_{2D}/I_G, are widely used for characterizing the defect density in graphitic materials. Both of the I_D/I_G and I_{2D}/I_G ratios show changes for different PWs and RFs, but the dominant changes are caused by the PW,

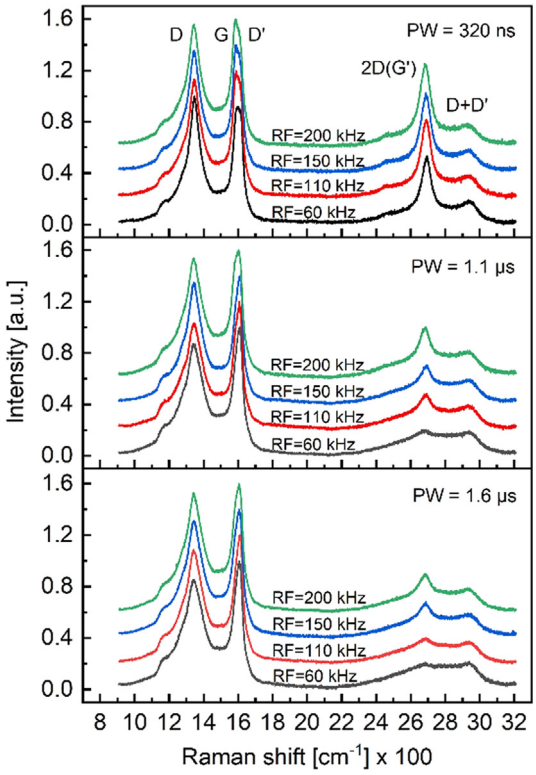

Fig. 3. Raman spectra of the samples synthesized from isopropanol by a bipolar PD with different PWs and RFs.

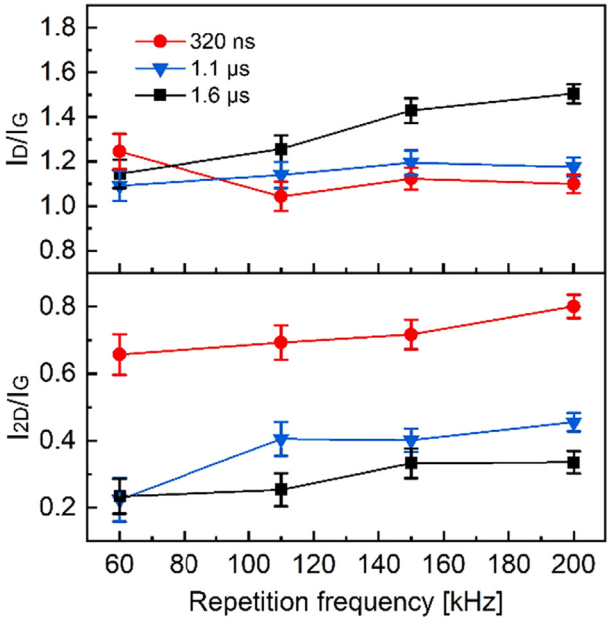

Fig. 4. Intensity ratios I_D/I_G and I_{2D}/I_G of the bands determined from the Raman spectra of the samples synthesized from isopropanol by a bipolar PD with different PWs and RFs.

while the RF has only a minor influence on both ratios. Samples prepared with PW = 320 ns exhibit a reduction of the I_D/I_G and a significant increase of the I_{2D}/I_G ratio.

The I_D/I_G intensity ratio of the D and G bands can be used to determine the average distance between defects L_D in graphene, following formula (1) [45,50]:

$$L_D = (12.0 \pm 6.3)\cdot\left(\frac{I_D}{I_G}\right)^{-0.5} nm \quad (1)$$

for an excitation wavelength of the laser of 532 nm. The average distance between defects is highest for the samples processed with PW = 320 ns and higher RFs, and it was calculated to be L_D = 11.5(6.0) nm. This means that the products prepared with short PWs and higher RFs are already in the area of small defect density [50].

The average number of stacked layers of graphene can be estimated from the ratio I_{2D}/I_G of band intensities. Namely, I_{2D}/I_G = 2 for pristine graphene, equals 1 for two layers and becomes 0 for graphite [46,50]. It was also reported that the position of the 2D(G′) band shifts to lower frequencies when the number of stacked graphene planes decreases [51]. Fig. 4 shows that the I_{2D}/I_G ratio increases for shorter PWs and higher RFs, thus the number of stacked graphene layers decreases. Furthermore, a shift of the 2D(G′) band to lower wavenumbers was observed with shorter PWs and higher RFs, confirming a decrease of the number of stacked graphene layers. The Raman spectra of the samples prepared with PW = 320 ns show a significant increase of the I_{2D}/I_G band ratio, as well as a reduction of the 2D(G′) band wavenumber from 2691 cm^{-1} to 2684 cm^{-1} with an increasing RF.

The evolution of the product can also be directly observed in the HRTEM images of different samples. Fig. 5 presents exemplary images of the samples obtained with different pulse widths and repetition frequencies. For long PWs and small RFs, Fig. 5(a), the product is dominated by more amorphous or strongly wrinkled carbonaceous structures. Shortening of the PW to 1.1 μs and increasing the RF to 110 kHz already shows increased formation of typical layered structures which are shown in Fig. 5(b). The sample prepared with PW = 320 ns and RF = 150 kHz, Fig. 5(c), is dominated by few layer graphene structures. These HRTEM observations correspond well with the evolution of the Raman spectra presented in Fig. 3.

3.2. Synthesis of nanographite

Exemplary TEM images of the local structure of the sample prepared with 3 min long bipolar PD in isopropanol, with PW = 320 ns and RF = 150 kHz, are presented in Fig. 6. Fig. 6(a) shows that the product of the synthesis is composed of agglomerates containing small carbon flakes and sheets creating multilayered structures. These structures are shown in detail in Fig. 6(b) and (c), where continuous graphene-type layers can be clearly identified, having typically 3–13 layers. The average interlayer spacing, obtained from more than 190 sites, was determined to be 3.4(0.3) Å, which is characteristic for graphite and few layer graphene [24]. Furthermore, electron diffraction showed diffraction rings corresponding to lattice distances d_1 = 3.35(0.07) Å, d_2 = 2.08(0.05) Å and d_3 = 1.21(0.05) Å. The observed lattice distances correspond well to the crystallographic planes (0 0 2), (1 0 1) and (1 1 0) of graphite, as reported elsewhere [52].

At this point, it is worth to mention that graphite nanoplates, graphite nanosheets and graphite nanoflakes have been defined to be characteristic of a thickness and/or lateral dimension less than 100 nm. Few-layer graphene contains a number of layers from 2 to about 5. Multi-layer graphene has been defined as a 2D sheet-like material consisting of small number between 2 and about 10 countable, stacked graphene layers of extended lateral dimension [53]. Since the product obtained with PW = 320 ns and RF = 150 kHz contains a mixture of few-layer (2–5 layers), multilayer graphene, and graphite nanosheets, it should be referred to as nanographite - a mixture of all these quantities, with a certain size distribution.

Additionally, nanometer-sized nanoparticles were found to be present in the material, Fig. 6(b) and (c). These nanoparticles, with an average diameter of 2.59(0.64) nm, are distributed homogeneously and contain mainly Mo and a smaller amount of W. These nanoparticles have been detected in every tested sample and they are likely impurities released from the electrodes caused by the mass transport during the electric discharges.

3.3. Influence of process time on product characteristics

To investigate the influence of the processing time on the structure of the samples and the yield of the synthesis, samples were prepared by applying the same conditions, but with different processing times. Fig. 7 shows the Raman spectra of the samples synthesized with PW = 320 ns, RF = 150 kHz and with processing times ranging from 1 to 15 min. It is apparent that no significant changes occur in the spectra, meaning that the processing time does not significantly influence the quality of the product. Nevertheless, minor differences of the spectra observed in Fig. 7 could be associated with local inhomogeneities in the tested batches. The yield of the product depending on the processing time is shown in Fig. 8. This dependence can be divided into 3 characteristic regions. First, the yield increases with a rate of ~69 $mg\cdot l^{-1}\cdot min^{-1}$. For processing times between 5 and 6 min, production rate increases significantly to ~282 $mg\cdot l^{-1}\cdot min^{-1}$. It is worth mentioning that dark fumes accompanied by a black precipitate in the vacuum chamber were observed for processing times longer than 4.5 min. This fuming is most likely caused by local heating at the plasma-liquid interface. As a result, the production rate for processing times over 6 min decreases to ca. 25 $mg\cdot l^{-1}\cdot min^{-1}$. Production rates are likely to be improved by means of an advanced reactor design with more effective cooling.

3.4. Investigations into possible reaction pathways

The synthesis of nanographite from isopropanol by plasma in liquid method can proceed in two possible reaction pathways. In the first, isopropanol is decomposed to carbon by hydrocarbon cracking and further on graphitization and reduction processes take place in the presence of hydrogen (top down). Along the second pathway,

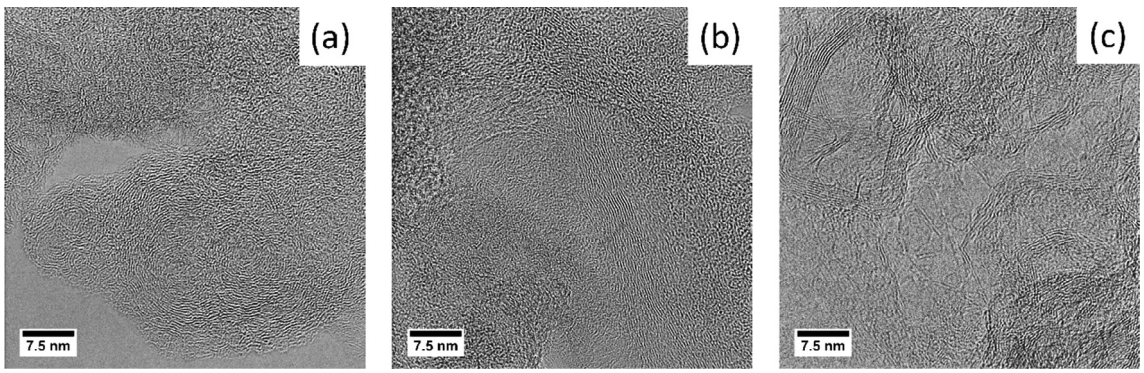

Fig. 5. HRTEM images of samples synthesized from isopropanol by the PiL method with different PWs and RFs: (a) PW = 1.6 μs and RF = 60 kHz, (b) PW = 1.1 μs and RF = 110 kHz, and (c) PW = 320 ns and RF = 150 kHz.

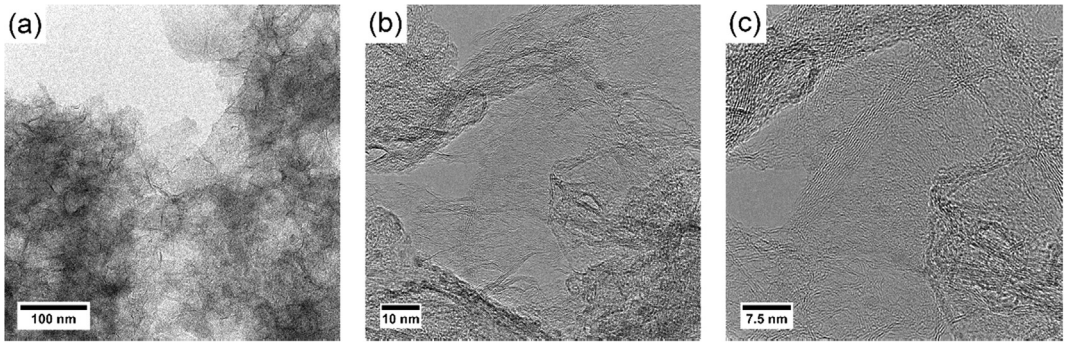

Fig. 6. Bright field TEM images of the sample synthesized from isopropanol by the PiL method with PW = 320 ns and RF = 150 kHz: (a) an overview of the observed structures, (b) and (c) high resolution images showing particular carbon layers.

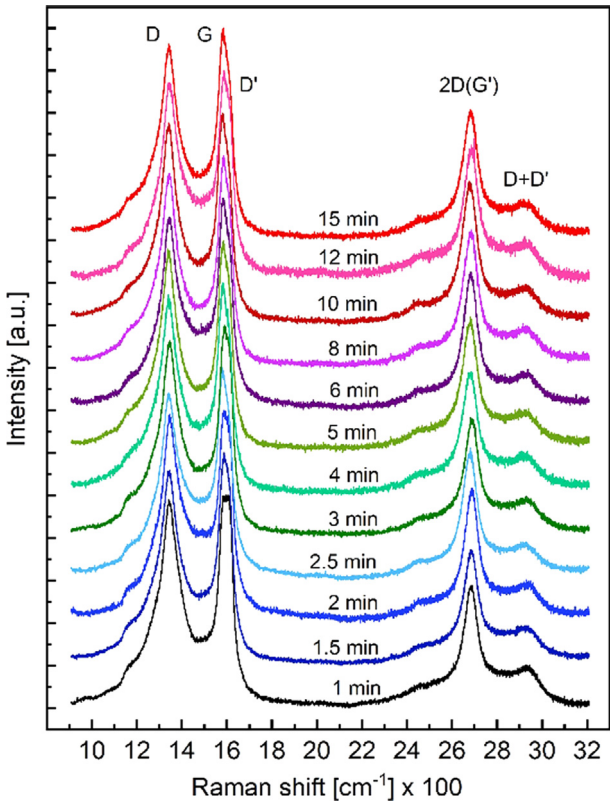

Fig. 7. Raman spectra of the samples synthesized with PW = 320 ns, RF = 150 kHz and with different processing times.

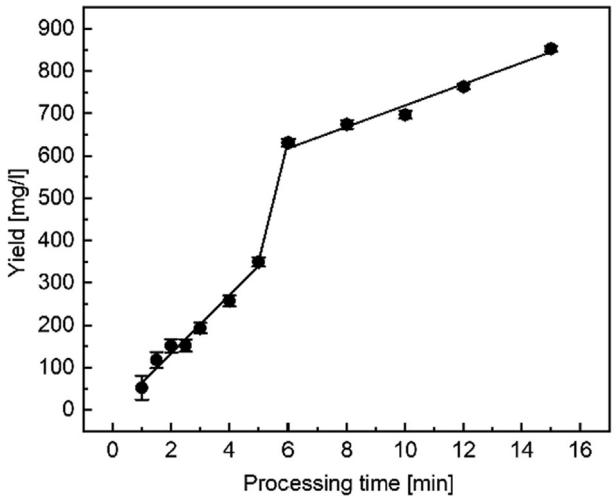

Fig. 8. Yield vs. processing time for the samples synthesized at PW = 320 ns and RF = 150 kHz with different processing times.

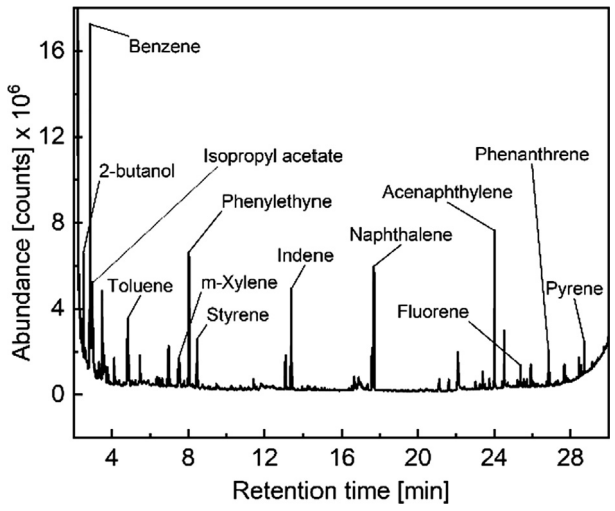

Fig. 9. Exemplary chromatogram of the filtrate obtained with PW = 320 ns and RF = 150 kHz. The identified byproducts of the synthesis are marked.

hydrocarbons are fragmented and then recombine to aliphatic, cyclic and aromatic compounds (bottom up). The presented results so far cannot confirm either one of these pathways. However, GC–MS results may provide guidance, which mechanism dominates during PiL synthesis of carbon nanostructures for different operating conditions.

Liquid samples obtained by filtration of the suspensions after the plasma treatment at different experimental conditions, namely PW and RF, were analyzed by GC–MS. Fig. 9 presents an exemplary chromatogram of the solution obtained with PW = 320 ns and RF = 150 kHz. Fig. 10 presents the main byproducts and their content detected in filtrates processed for 3 min with RF = 150 kHz and different pulse durations.

Fig. 10 shows the content of the liquid hydrocarbon byproducts resulting from the PiL synthesis applying RF = 150 kHz and different PWs. Here, it is worth mentioning that the content shown in Fig. 10 can be interpreted as the ratio of by-products of the synthesis with respect to each other, without an information about the ratio of the by-products to the precursor. The ratio of the by-products to the precursor lies in the ppm regime, and at this stage of the research, it can only be treated as an indication of the reaction mechanisms.

The hydrocarbon precursor is first broken up in fragments (e.g. 2-butanol, isopropyl acetate) which then combine into more complex products, in particular into ring structures (e.g. benzene, toluene, phenylethylene, etc.). The dominance especially of isopropyl acetate,

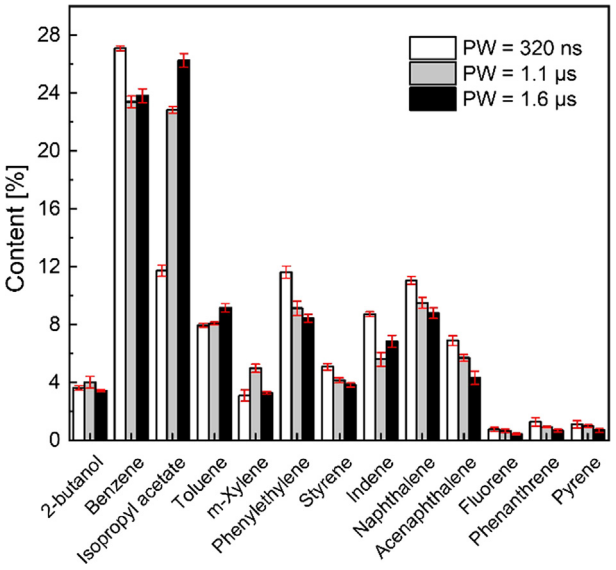

Fig. 10. Content of the byproducts detected in the liquids processed with RF = 150 kHz and with different pulse widths.

together with a relatively small yield of more complex compounds, for longer pulses suggests that although these conditions were suitable to promote fragmentation, they were not sufficient to drive the formation of complex ring structures. Conversely, shorter pulses of 320 ns resulted in significantly higher concentrations of aromatic compounds such as phenylethyne, styrene, indene, naphthalene, acenaphthylene, fluorene, phenanthrene or pyrene concurrent with a relative decrease in concentrations of simpler molecules, foremost isopropyl acetate, which have apparently been consumed in the associated syntheses. This means that ring closure and condensation to benzene and toluene, as well as to poly-aromatic systems such as indene, naphthalene or acenaphthylene, are promoted.

The kinetics of the multiple chemical reactions that can occur in solution during the PiL process is quite complicated. What is presented here is only a first qualitative analysis of the by-products present in the liquid phase. A detailed investigation of the relation between plasma operation parameters, e.g. electron densities and temperatures, and specific steps and mechanisms in the synthesis of nanographite from aliphatic precursors is an interesting challenge. The respective findings would provide crucial information to further improve the process and drive the commercial implementation as an efficient and environmental benign method.

4. Summary

A novel and fast plasma-in-liquid method was applied to synthesize nanographite structures from isopropanol by bipolar pulsed electric discharges with short pulse lengths down to the nanoseconds and high repetition frequencies in the kilohertz regime. Systematic studies demonstrated that the pulse width and the repetition frequency have a significant influence on the quality of the product. Short pulse widths and high repetition frequencies lead to an increase of the energy density of the plasma in liquid and therefore to fast reduction processes and the formation of few layer graphene.

Long pulses and low repetition frequencies promote the creation of isopropyl acetate, meaning that the plasma conditions are not suited to drive the formation of complex carbon ring structures required to build graphene layers. Hydrocarbon cracking followed by graphitization already occur, but the plasma conditions are not suitable to drive the reduction processes. In contrast, short pulses and high repetition frequencies lead to significantly higher concentration of poly-aromatic compounds, showing that ring closure and condensation to benzene, toluene and other poly-aromatic systems are promoted. Higher energy density of the plasma in liquid also ensures fast reduction processes in the presence of hydrogen and formation of nanographite.

Few layer graphene with an average interlayer spacing of 3.4(0.3) Å was synthesized applying electric pulses characteristic of PW = 320 ns and RF = 150 kHz. The average distance between defects L_D, determined from the I_D/I_G intensity ratio of the D and G bands in the Raman spectra, is maximal for samples processed with PW = 320 ns, and it was estimated to be 11.5(6.0) nm. No significant influence on the product was observed for different discharge times. Nevertheless, the yield increased significantly after approximately 4.5 min of discharge when a dark fuming was observed. The presented results show that this cost efficient and environmentally benign single-step-method can rapidly produce nanographite or few layer graphene with small defect densities.

CRediT authorship contribution statement

W. Bodnar: Conceptualization, Methodology, Validation, Formal analysis, Investigation, Writing - original draft, Writing - review & editing, Visualization. **M. Schiorlin:** Methodology, Validation, Formal analysis, Investigation, Writing - original draft. **A. Frank:** Formal analysis, Investigation, Writing - original draft. **T. Schulz:** Investigation, Writing - original draft. **N. Wöhrl:** Methodology, Writing - original draft. **C. Miron:** Conceptualization, Investigation, Writing - original draft. **C. Scheu:** Methodology, Formal analysis, Writing - original draft. **J.F. Kolb:** Conceptualization, Validation, Writing - original draft. **A. Kruth:** Conceptualization, Validation, Formal analysis, Writing - original draft, Project administration, Funding acquisition.

Declaration of Competing Interest

The authors declare that they have no known competing financial interests or personal relationships that could have appeared to influence the work reported in this paper.

Acknowledgements

This work was supported by the German Federal Ministry for Economic Affairs and Energy (Project No. 16KN 045245), within the framework of the AiF Network BiS Net - Brennstoffzellen in Serie. We would also like to thank Jens Wartmann (The Hydrogen and Fuel Cell Center ZBT GmbH) and Ronny Brandenburg (Leibniz Institute for Plasma Science and Technology) for their invaluable support and fruitful discussions.

References

[1] R. Mertens, The Graphene Handbook (2019 Edition), 2019, Lulu. com.
[2] A.M. Dimiev, S. Eigler, Graphene Oxide: Fundamentals and Applications, John Wiley & Sons, 2016.
[3] M.F. De Volder, et al., Carbon nanotubes: present and future commercial applications, Science 339 (6119) (2013) 535–539.
[4] Y. Zhu, et al., Graphene and graphene oxide: synthesis, properties, and applications, Adv. Mater. 22 (35) (2010) 3906–3924.
[5] M.J. Allen, V.C. Tung, R.B. Kaner, Honeycomb carbon: a review of graphene, Chem. Rev. 110 (1) (2010) 132–145.
[6] P. Avouris, C. Dimitrakopoulos, Graphene: synthesis and applications, Mater. Today 15 (3) (2012) 86–97.
[7] A. Alsaeedi, Y. Show, Synthesis of nano-carbon by in-liquid plasma method and its application to a support material of Pt catalyst for fuel cell, Nanomater. Nanotechnol. 9 (2019) 1847980419853159.
[8] V. Gamaleev, et al., Investigation of nanographene produced by in-liquid plasma for development of highly durable polymer electrolyte fuel cells, C–J. Carbon Res. 4 (4) (2018) 65.
[9] M. Peplow, Graphene: the quest for supercarbon, Nat. News 503 (7476) (2013) 327.
[10] K.S. Novoselov, et al., Electric field effect in atomically thin carbon films, Science 306 (5696) (2004) 666–669.
[11] E. Rollings, et al., Synthesis and characterization of atomically thin graphite films on a silicon carbide substrate, J. Phys. Chem. Solids 67 (9–10) (2006) 2172–2177.
[12] C. Virojanadara, et al., Homogeneous large-area graphene layer growth on 6 H-SiC

(0001), Phys. Rev. B 78 (24) (2008) 245403.
[13] C. Vallés, et al., Solutions of negatively charged graphene sheets and ribbons, J. Am. Chem. Soc. 130 (47) (2008) 15802–15804.
[14] P. Blake, et al., Graphene-based liquid crystal device, Nano Lett. 8 (6) (2008) 1704–1708.
[15] Y. Hernandez, et al., High-yield production of graphene by liquid-phase exfoliation of graphite, Nat. Nanotechnol. 3 (9) (2008) 563.
[16] J. Wang, et al., Free-standing subnanometer graphite sheets, Appl. Phys. Lett. 85 (7) (2004) 1265–1267.
[17] A. Dato, et al., Substrate-free gas-phase synthesis of graphene sheets, Nano Lett. 8 (7) (2008) 2012–2016.
[18] H.C. Schniepp, et al., Functionalized single graphene sheets derived from splitting graphite oxide, J. Phys. Chem. B 110 (17) (2006) 8535–8539.
[19] K. Subrahmanyam, et al., A study of graphenes prepared by different methods: characterization, properties and solubilization, J. Mater. Chem. 18 (13) (2008) 1517–1523.
[20] O.E. Andersson, et al., Structure and electronic properties of graphite nanoparticles, Phys. Rev. B 58 (24) (1998) 16387.
[21] A. Reina, et al., Large area, few-layer graphene films on arbitrary substrates by chemical vapor deposition, Nano Lett. 9 (1) (2008) 30–35.
[22] A. Münzer, et al., All gas-phase synthesis of graphene: Characterization and its utilization for silicon-based lithium-ion batteries, Electrochim. Acta 272 (2018) 52–59.
[23] L. Zhu, et al., High-quality production of graphene by liquid-phase exfoliation of expanded graphite, Mater. Chem. Phys. 137 (3) (2013) 984–990.
[24] F. Rozploch, J. Patyk, J. Stankowski, Graphenes bonding forces in graphite, Acta Phys. Pol. A 112 (2007) 557.
[25] J. Texter, Graphene dispersions, Curr. Opin. Colloid Interface Sci. 19 (2) (2014) 163–174.
[26] X. Wang, et al., Large-scale synthesis of few-layered graphene using CVD, Chem. Vap. Deposition 15 (1–3) (2009) 53–56.
[27] N. Woehrl, et al., Plasma-enhanced chemical vapor deposition of graphene on copper substrates, AIP Adv. 4 (4) (2014) 047128.
[28] K.V. Emtsev, et al., Towards wafer-size graphene layers by atmospheric pressure graphitization of silicon carbide, Nat. Mater. 8 (3) (2009) 203.
[29] V. Presser, M. Heon, Y. Gogotsi, Carbide-derived carbons–from porous networks to nanotubes and graphene, Adv. Funct. Mater. 21 (5) (2011) 810–833.
[30] N. Parveen, M.O. Ansari, M.H. Cho, Simple route for gram synthesis of less defective few layered graphene and its electrochemical performance, RSC Adv. 5 (56) (2015) 44920–44927.
[31] K. Parvez, et al., Exfoliation of graphite into graphene in aqueous solutions of inorganic salts, J. Am. Chem. Soc. 136 (16) (2014) 6083–6091.
[32] S. Horikoshi, N. Serpone, In-liquid plasma: a novel tool in the fabrication of nanomaterials and in the treatment of wastewaters, RSC Adv. 7 (75) (2017) 47196–47218.
[33] Q. Chen, J. Li, Y. Li, A review of plasma–liquid interactions for nanomaterial synthesis, J. Phys. D Appl. Phys. 48 (2015) 424005.
[34] G. Saito, T. Akiyama, Nanomaterial synthesis using plasma generation in liquid, J. Nanomater. 2015 (2015) 1–21.
[35] M. Matsushima, et al., Formation of graphene nano-particle by means of pulsed discharge to ethanol, J. Appl. Phys. 113 (11) (2013).
[36] T. Hagino, et al., Ultrahigh-speed synthesis of nanographene using alcohol in-liquid plasma, Appl. Phys Express 5 (3) (2012).
[37] S. Kim, et al., Production of Graphite Nanosheets by Low-Current Plasma Discharge in Liquid Ethanol, Mater. Trans. 51 (8) (2010) 1455–1459.
[38] Z. Chen, et al., Rapid formation of diamond-like nano-carbons in a gas bubble discharge in liquid ethanol, Plasma Chem. Plasma Process. 38 (1) (2018) 75–87.
[39] C.-S. Park, et al., Simple one-step synthesis of carbon nanoparticles from aliphatic alcohols and n-hexane by stable solution plasma process, Carbon Letters (Carbon Lett.) 28 (2018) 31–37.
[40] Hori, M., et al. High-speed synthesis and crystalinity control of nanographene using in-liquid plasma in alcohol, in: ESCAMPIG XXI, Viana do Castelo, Portugal, 2012.
[41] S. Kim, et al., Production of graphite nanosheets by low-current plasma discharge in liquid ethanol, Mater. Trans. (2010) 1007121116–1007121116.
[42] R. Sergiienko, et al., Structure of graphite nanosheets formed by plasma discharge in liquid ethanol, Powder Metall. Met. Ceram. 52 (5–6) (2013) 278–290.
[43] D.Z. Pai, Nanomaterials synthesis at atmospheric pressure using nanosecond discharges, J. Phys. D Appl. Phys. 44 (17) (2011).
[44] I. Childres, et al., Raman spectroscopy of graphene and related materials, in: New developments in photon and materials research, 2013.
[45] A.C. Ferrari, Raman spectroscopy of graphene and graphite: Disorder, electron–phonon coupling, doping and nonadiabatic effects, Solid State Commun. 143 (1–2) (2007) 47–57.
[46] A.C. Ferrari, et al., Raman spectrum of graphene and graphene layers, Phys Rev Lett 97 (18) (2006) 187401.
[47] M. Pimenta, et al., Studying disorder in graphite-based systems by Raman spectroscopy, Phys. Chem. Chem. Phys. 9 (11) (2007) 1276–1290.
[48] M.S. Dresselhaus, et al., Perspectives on carbon nanotubes and graphene Raman spectroscopy, Nano Lett 10 (3) (2010) 751–758.
[49] V. Sharma, et al., Structure and chemistry of crankcase and exhaust soot extracted from diesel engines, Carbon 103 (2016) 327–338.
[50] L.G. Cancado, et al., Quantifying defects in graphene via Raman spectroscopy at different excitation energies, Nano Lett. 11 (8) (2011) 3190–3196.
[51] L. Cançado, et al., Geometrical approach for the study of G′ band in the Raman spectrum of monolayer graphene, bilayer graphene, and bulk graphite, Phys. Rev. B 77 (24) (2008) 245408.
[52] R.W.G. Wyckoff, Crystal Structures, second ed., vol. 1., Interscience Publishers, Inc., New York, 1963.
[53] A. Bianco, et al., All in the graphene family–A recommended nomenclature for two-dimensional carbon materials, Elsevier, 2013.